[Journal of Geophysical Research: Solid Earth]

Supporting Information for

Fine structure of tremor migrations beneath the Kii Peninsula, Southwest Japan, extracted with a space-time Hough transform

Kodai Sagae[1,2]*, Hisashi Nakahara[1], Takeshi Nishimura[1], and Kazutoshi Imanishi[3]

[1]Department of Geophysics, Graduate School of Science, Tohoku University, 6-3, Aramaki Aza-Aoba, Aoba-ku, Sendai, Miyagi, 980-8578, Japan.

[2]Now at Geological Survey of Japan, National Institute of Advanced Industrial Science and Technology (AIST), Tsukuba Central 7, 1-1-1 Higashi, Tsukuba, Ibaraki, 305-8567, Japan.

[3]Geological Survey of Japan, National Institute of Advanced Industrial Science and Technology (AIST), Tsukuba Central 7, 1-1-1 Higashi, Tsukuba, Ibaraki, 305-8567, Japan.

Contents of this file

Additional Supporting Information (Files uploaded separately)

Captions for Data Set S1

Introduction

This supplement contains the followings. The derivation of a space-time Hough transform (Equation 1) in the main text is detailed in Text S1. Figures S2–S12 show tremor migrations extracted in all tremor episodes from July 2012 to July 2014. Figure S13 shows spatial patterns of tremor migrations with high speeds (10 km/hr or more). Figure S14 shows spatial distribution of RTRs during tremor episodes. Data Set S1 is the catalog of tremor migrations extracted in the present study.

Text S1. Derivation of space-time Hough transform

This section explains the derivation of Equation 1 in the main text. We consider (x, y, t) as a coordinate of a tremor event, where x is the longitude (the east is positive), y is the latitude (the north is positive), and t is the detection time. We want to express a tremor migration as a straight line in a (2+1)-D space-time (2-D in space and 1-D in time). In addition, information on uncertainties of tremor locations is taken into account by giving spatial spread to the straight line (by considering a cylinder). We use tyt-Euler angle to represent an arbitrary position of the cylinder in the (2+1)-D space-time. The tyt-Euler angle is rotations of coordinate system in the following order (Figures S1a–1c), rotating the system (x, y, t) around the t-axis by ϕ, rotating the system $(x^{(1)}, y^{(1)}, t)$ around the rotated y-axis ($y^{(1)}$-axis) by θ, and then rotating the system $(x^{(2)}, y^{(1)}, t^{(1)})$ around the rotated t-axis ($t^{(1)}$-axis) by ψ. Here, θ is the zenith angle, ϕ is the azimuth, and ψ is the rotation angle. We consider standard unit vectors in ordinal coordinate system as $\overrightarrow{e_x}$, $\overrightarrow{e_y}$ and $\overrightarrow{e_t}$. As shown in Figure S1a, standard unit vectors in the rotated coordinate system ($x^{(1)}, y^{(1)}$, and t) around the t-axis by ϕ are represented as:

$$\begin{aligned} \overrightarrow{e_x^{(1)}} &= \cos\phi\ \overrightarrow{e_x} + \sin\phi\ \overrightarrow{e_y} \\ \overrightarrow{e_y^{(1)}} &= -\sin\phi\ \overrightarrow{e_x} + \cos\phi\ \overrightarrow{e_y} \\ & \qquad \overrightarrow{e_t}, \end{aligned} \tag{S1}$$

where $\overrightarrow{e_x^{(1)}}$, and $\overrightarrow{e_y^{(1)}}$ are standard unit vectors after the rotation by ϕ. Next, as shown in Figure S1b, standard unit vectors in the rotated coordinate system ($x^{(2)}, y^{(1)}$, and $t^{(1)}$) around the rotated y-axis ($y^{(1)}$-axis) by θ are represented as:

$$\begin{aligned} \overrightarrow{e_x^{(2)}} &= \cos\theta\ \overrightarrow{e_x^{(1)}} - \sin\theta\ \overrightarrow{e_t} \\ & \qquad \overrightarrow{e_y^{(1)}} \\ \overrightarrow{e_t^{(1)}} &= \sin\theta\ \overrightarrow{e_x^{(1)}} + \cos\theta\ \overrightarrow{e_t}, \end{aligned} \tag{S2}$$

where $\overrightarrow{e_x^{(2)}}$ and $\overrightarrow{e_t^{(1)}}$ are standard unit vectors after the rotation by θ. Notably, the vectors of $\overrightarrow{e_x^{(2)}}$, $\overrightarrow{e_y^{(1)}}$, and $\overrightarrow{e_t^{(1)}}$ are consistent with standard unit vectors in the polar coordinate system ($\overrightarrow{e_\theta}, \overrightarrow{e_\phi}, \overrightarrow{e_r}$), where $\overrightarrow{e_\theta} = (\cos\theta\cos\phi\,, \cos\theta\sin\phi\,, -\sin\theta)^T$, $\overrightarrow{e_\phi} = (-\sin\phi\,, \cos\phi, 0)^T$, and $\overrightarrow{e_r} = (\sin\theta\cos\phi, \sin\theta\sin\phi\,, \cos\theta)^T$. Finally, as shown in Figure S1c, standard unit vectors in the rotated coordinate system ($x^{(3)}, y^{(2)}$, and $t^{(1)}$) around the rotated t-axis ($t^{(1)}$-axis) by ψ are represented as:

$$\begin{aligned}\overrightarrow{e_x^{(3)}} &= \cos\psi\,\overrightarrow{e_x^{(2)}} + \sin\psi\,\overrightarrow{e_y^{(1)}} \\ \overrightarrow{e_y^{(2)}} &= -\sin\psi\,\overrightarrow{e_x^{(2)}} + \cos\psi\,\overrightarrow{e_y^{(1)}} \\ &\overrightarrow{e_t^{(1)}},\end{aligned} \tag{S3}$$

where $\overrightarrow{e_x^{(3)}}$ and $\overrightarrow{e_y^{(2)}}$ are standard unit vectors after the rotation by ψ. Summarizing Equations from S1 to S3,

$$\begin{aligned}\overrightarrow{e_x^{(3)}} &= \begin{pmatrix} -\sin\phi\sin\psi + \cos\theta\cos\phi\cos\psi \\ \cos\phi\sin\psi + \cos\theta\sin\phi\cos\psi \\ -\sin\theta\cos\psi \end{pmatrix} \\ \overrightarrow{e_y^{(2)}} &= \begin{pmatrix} -\sin\phi\cos\psi - \cos\theta\cos\phi\sin\psi \\ \cos\phi\cos\psi - \cos\theta\sin\phi\sin\psi \\ \sin\theta\sin\psi \end{pmatrix} \\ \overrightarrow{e_t^{(1)}} &= \begin{pmatrix} \sin\theta\cos\phi \\ \sin\theta\sin\phi \\ \cos\theta \end{pmatrix}.\end{aligned} \tag{S4}$$

The rotation matrix of the tyt-Euler angle is represented as:

$$R(\theta,\phi,\psi) = (\overrightarrow{e_x^{(3)}}\,\overrightarrow{e_y^{(2)}}\,\overrightarrow{e_t^{(1)}}) = (\vec{\alpha}\,\vec{\beta}\,\vec{\gamma}) = \begin{pmatrix} -\sin\phi\sin\psi + \cos\theta\cos\phi\cos\psi & -\sin\phi\cos\psi - \cos\theta\cos\phi\sin\psi & \sin\theta\cos\phi \\ \cos\phi\sin\psi + \cos\theta\sin\phi\cos\psi & \cos\phi\cos\psi - \cos\theta\sin\phi\sin\psi & \sin\theta\sin\phi \\ -\sin\theta\cos\psi & \sin\theta\sin\psi & \cos\theta \end{pmatrix}, \tag{S5}$$

where $R(\theta, \phi, \psi)$ is the rotation matrix of the tyt-Euler angle, $\vec{\alpha}$, $\vec{\beta}$, and $\vec{\gamma}$ are unit vectors of Equation 2 in the main text. If θ is equal to zero, the rotations of coordinate system by ϕ and ψ are operations around the same axis (t-axis). There is no problem in the present study because migration speed (=$\tan\theta$) is always larger than zero and the range of θ is $0° < \theta < 90°$.

We consider a cylinder whose cylindrical axis is located at (ρ, 0, 0) and its radius is r, where ρ is the distance from an origin to the cylindrical axis. The equation of the cylinder is represented as:

$$\begin{pmatrix} x \\ y \\ t \end{pmatrix} = \begin{pmatrix} \rho + r\cos\lambda \\ r\sin\lambda \\ m \end{pmatrix}, \tag{S6}$$

where λ and m are parameters related to the angle around the t-axis measured counterclockwise from the x-axis and the direction of the straight line (direction of cylindrical axis), respectively. An arbitrary position of the cylinder in the (2+1)-D space-time is represented by rotating Equation S6 using Equation S5:

$$\begin{pmatrix} x \\ y \\ t \end{pmatrix} = R(\theta, \phi, \psi) \begin{pmatrix} \rho + r\cos\lambda \\ r\sin\lambda \\ m \end{pmatrix} = (\rho + r\cos\lambda)\,\vec{\alpha} + (r\sin\lambda)\,\vec{\beta} + m\,\vec{\gamma}\,. \tag{S7}$$

Equation 1 in the main text is derived by calculating Equation S7.

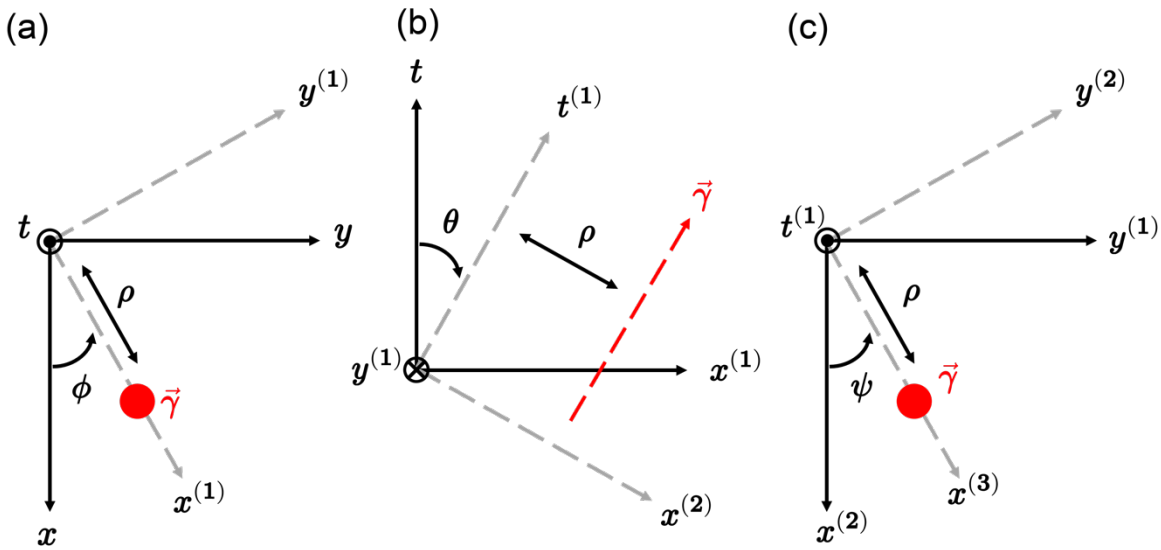

Figure S1. Schematic diagrams of tyt-Euler angle. (**a**) Rotation of coordinate system (x, y, t) around the t-axis by ϕ. (**b**) Rotation of the system ($x^{(1)}$, $y^{(1)}$, t) around the rotated y-axis ($y^{(1)}$-axis) by θ. (**c**) Rotation of the system ($x^{(2)}$, $y^{(1)}$, $t^{(1)}$) around the rotated t-axis ($t^{(1)}$-axis) by ψ. The red dots and arrow show locations of the unit direction vector (cylindrical axis) in rotation processes of the coordinate system.

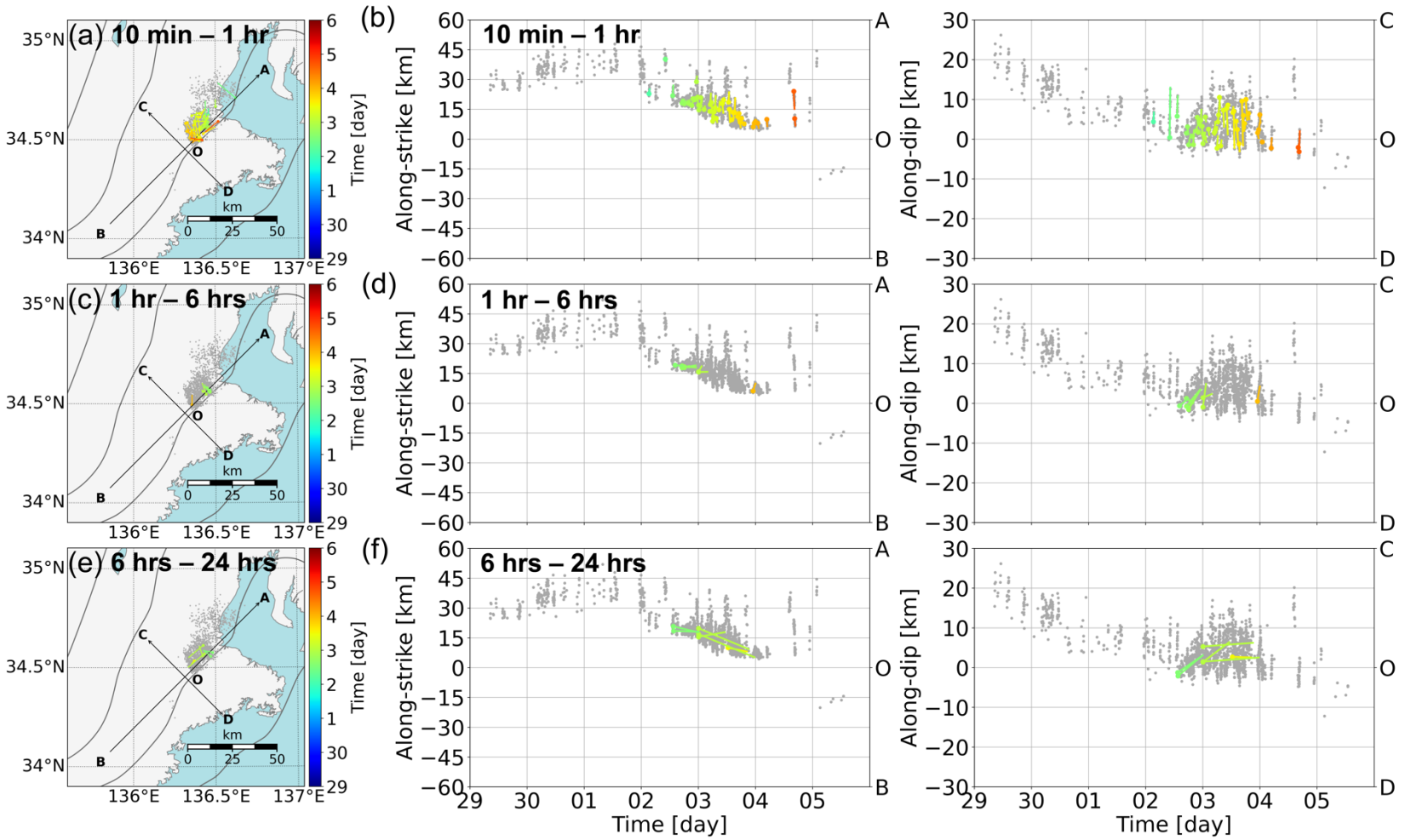

Figure S2. Tremor migrations during a tremor episode from September 29th to October 5th, 2012. (**a**) Map view of the tremor migrations with durations ranging from 10 min to 1 h. The gray dots show locations of tremors. Colored lines and dots show tremor migrations and their starting points, and the colors show the starting time of tremor migrations. (**b**) Spatiotemporal plots of the tremor

migrations with the same durations as that of (**a**). The left panel shows spatiotemporal evolutions of tremor migrations along the strike (A–B) and the right panel shows spatiotemporal evolutions of ones along the dip (C–D). (**c**), (**d**) Same as (**a**) and (**b**), but for tremor migrations with durations ranging from 1 h to 6 h. (**e**), (**f**) Same as (**a**) and (**b**), but for tremor migrations with durations ranging from 6 h to 24 h.

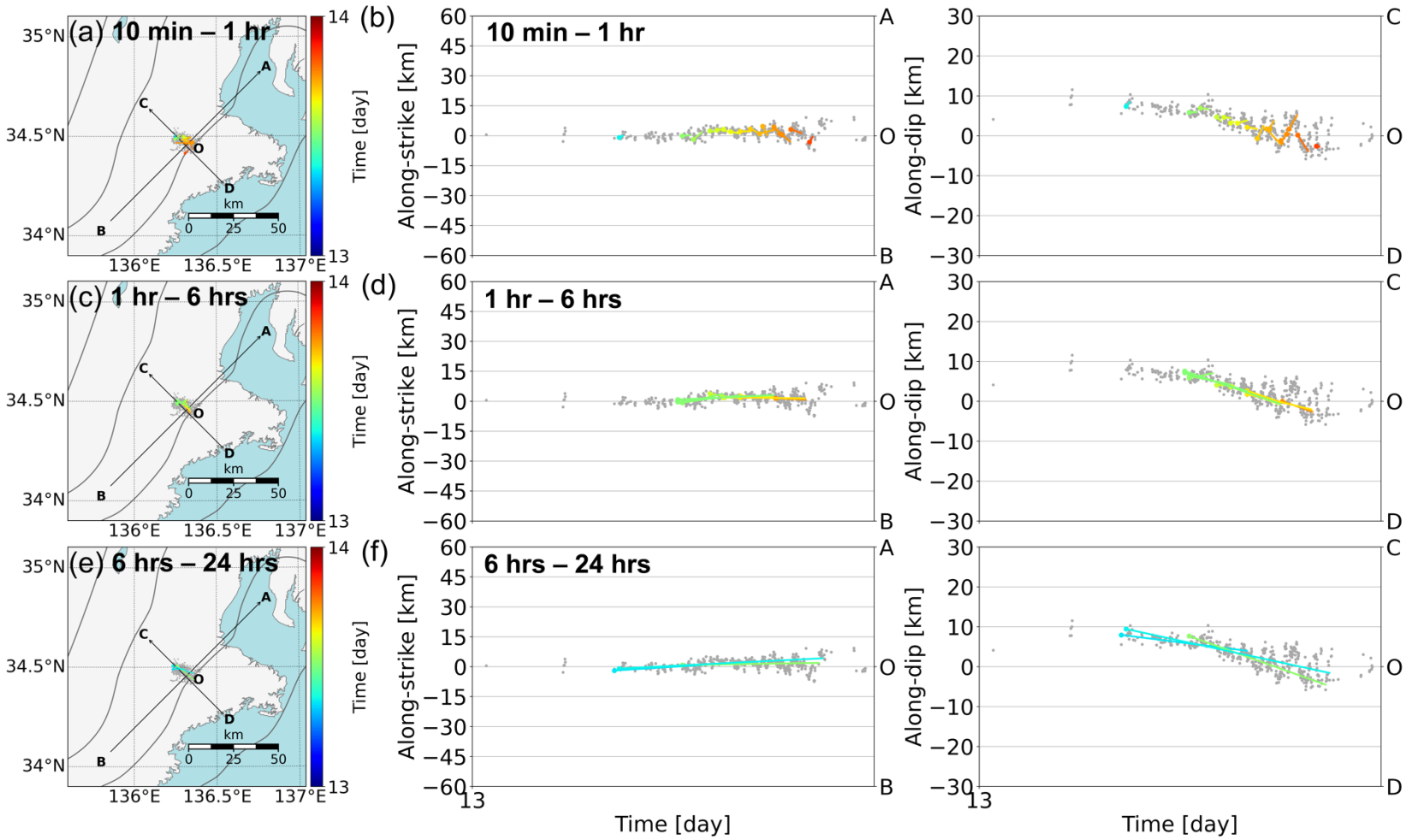

Figure S3. Same as Figure S2, but for tremor episode on December 13th, 2012.

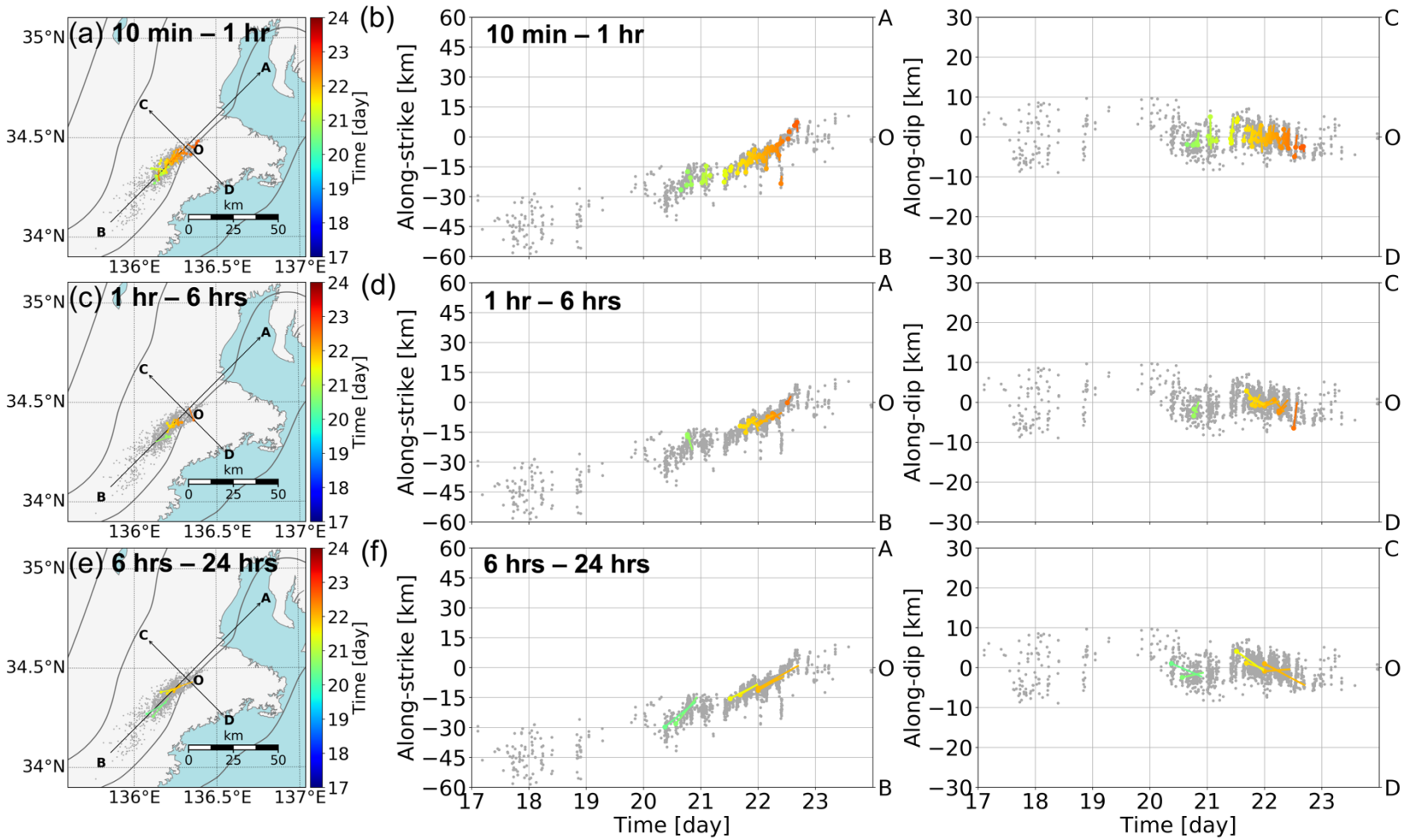

Figure S4. Same as Figure S2, but for tremor episode from December 17th to 23rd, 2012.

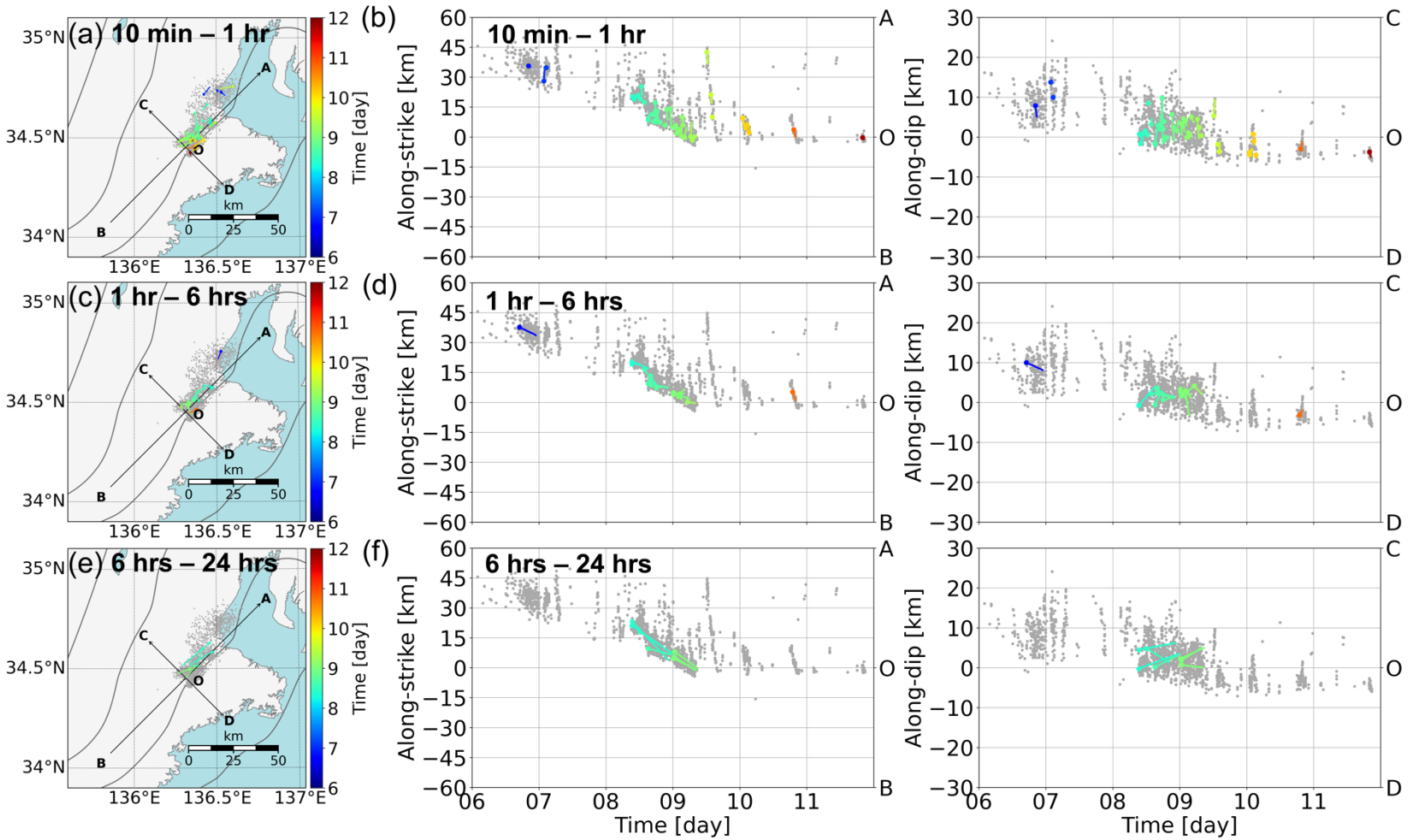

Figure S5. Same as Figure S2, but for tremor episode from April 6th to 11th, 2013.

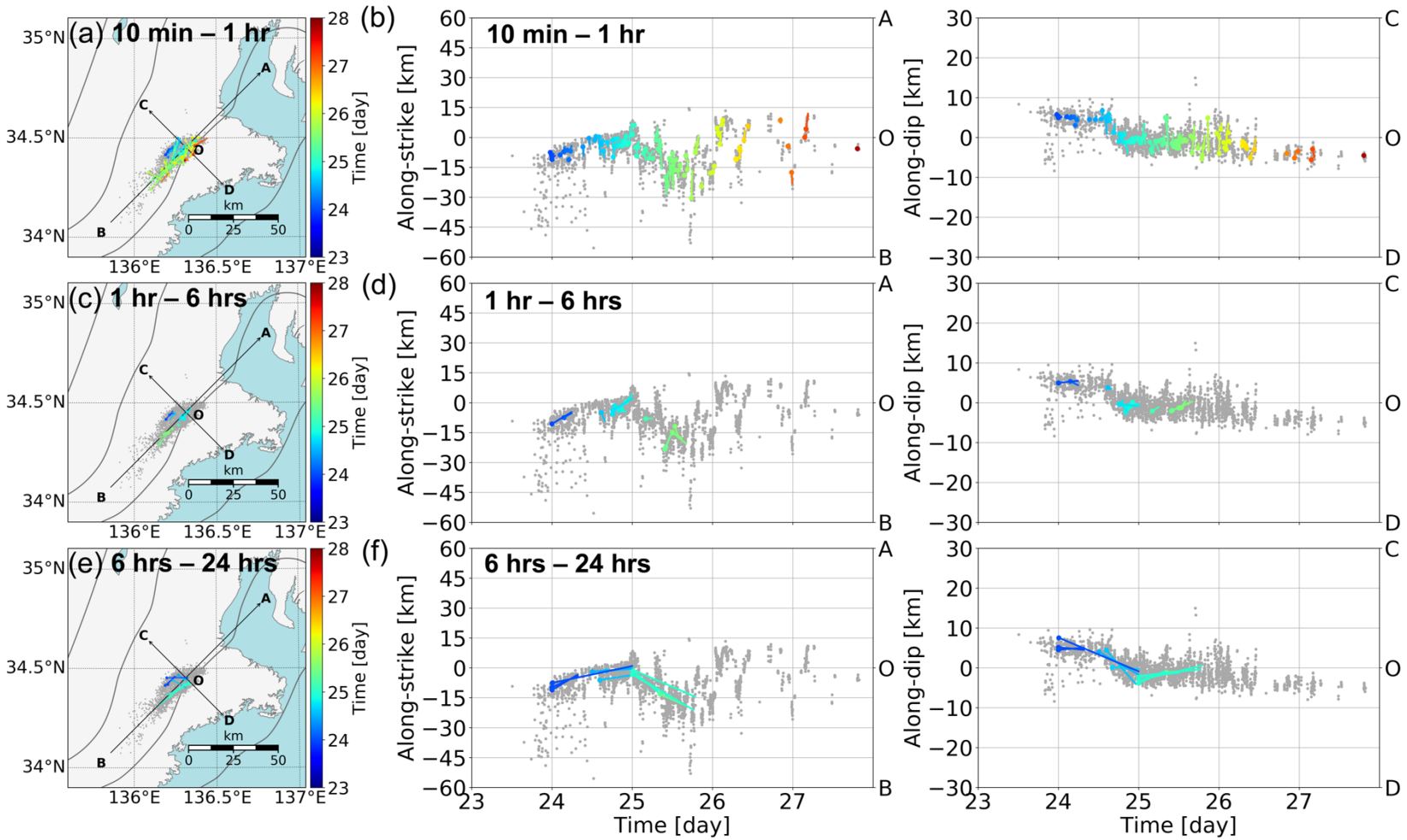

Figure S6. Same as Figure S2, but for tremor episode from July 23rd to 27th, 2013.

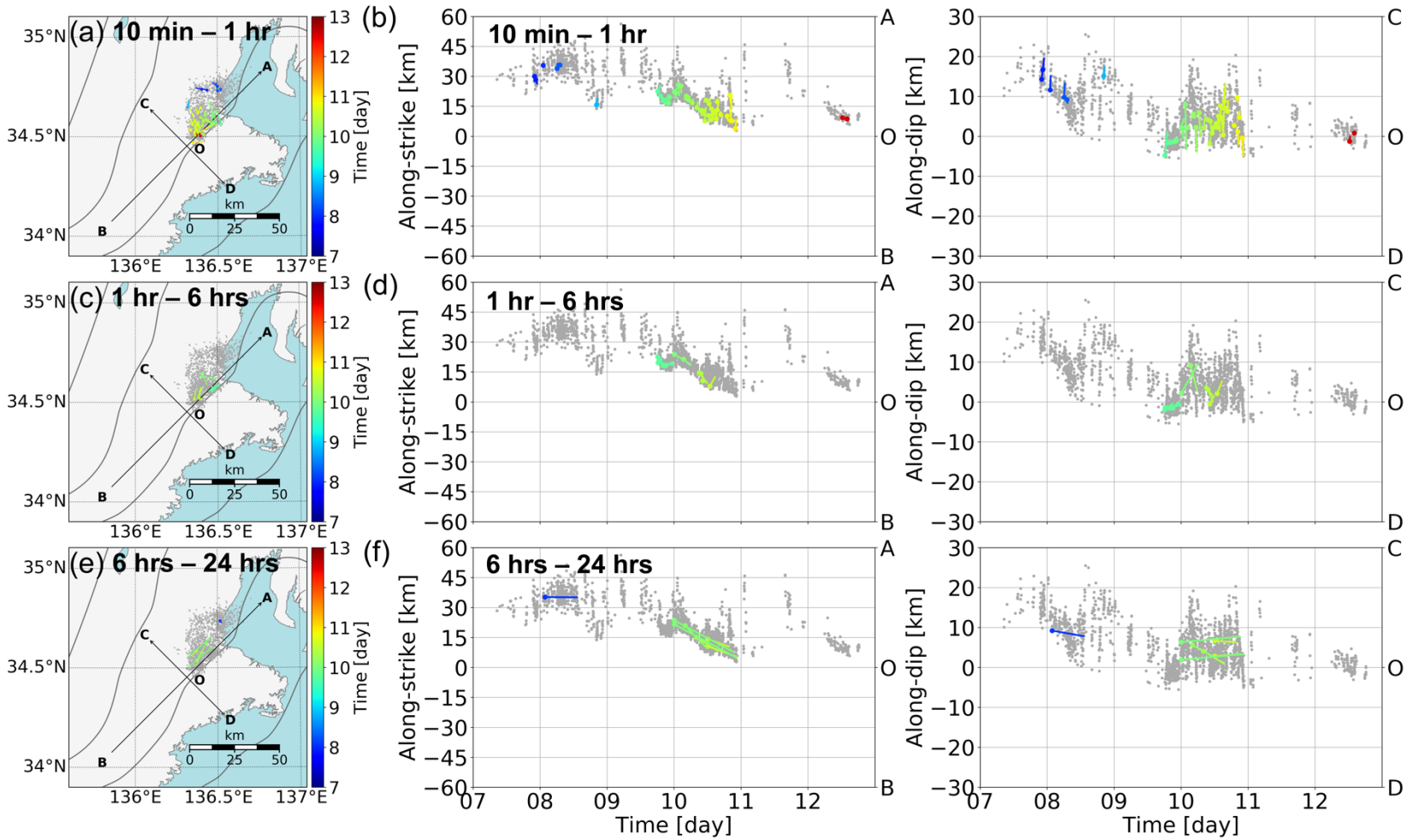

Figure S7. Same as Figure S2, but for tremor episode from September 7th to 12th, 2013.

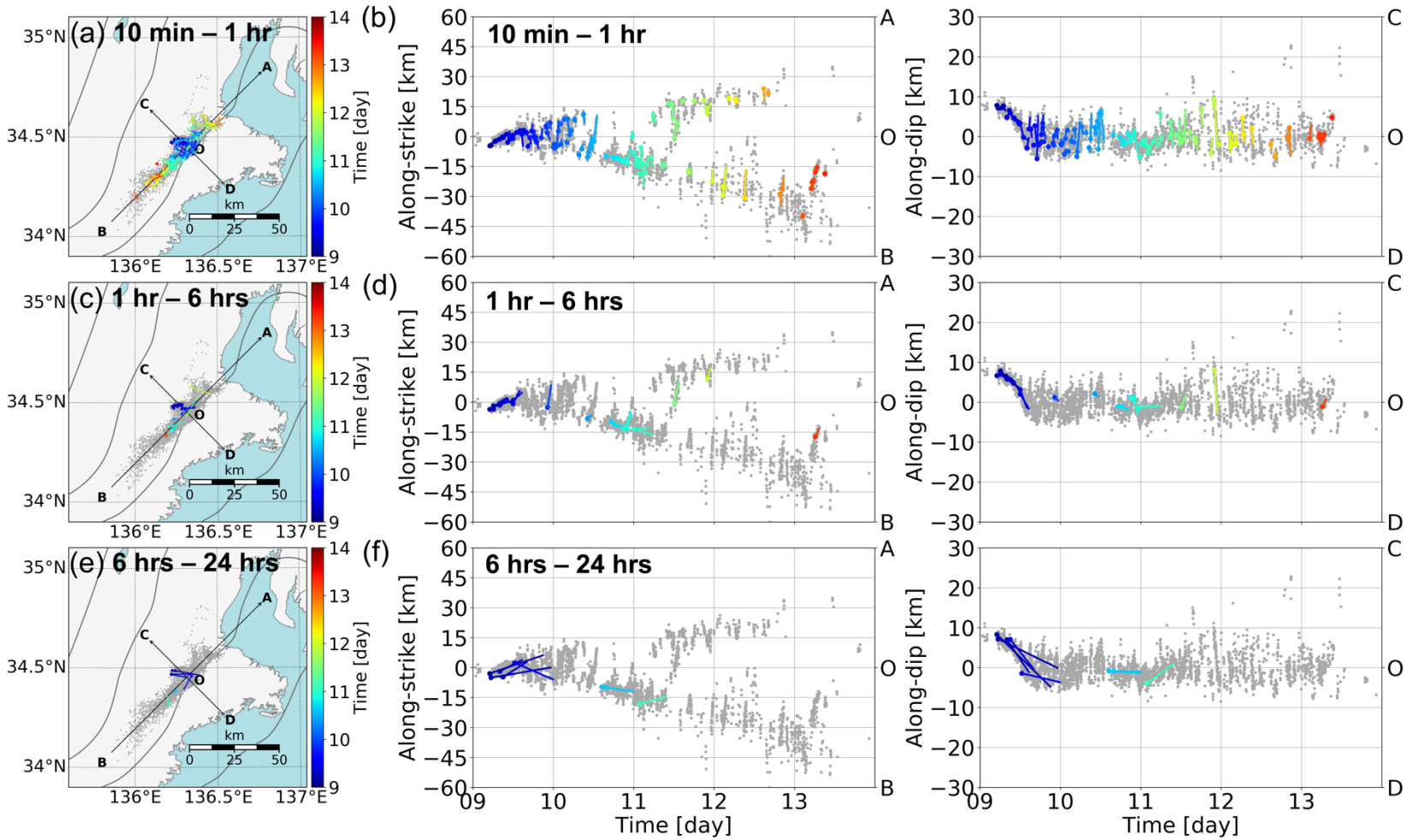

Figure S8. Same as Figure S2, but for tremor episode from January 9th to 13th, 2014.

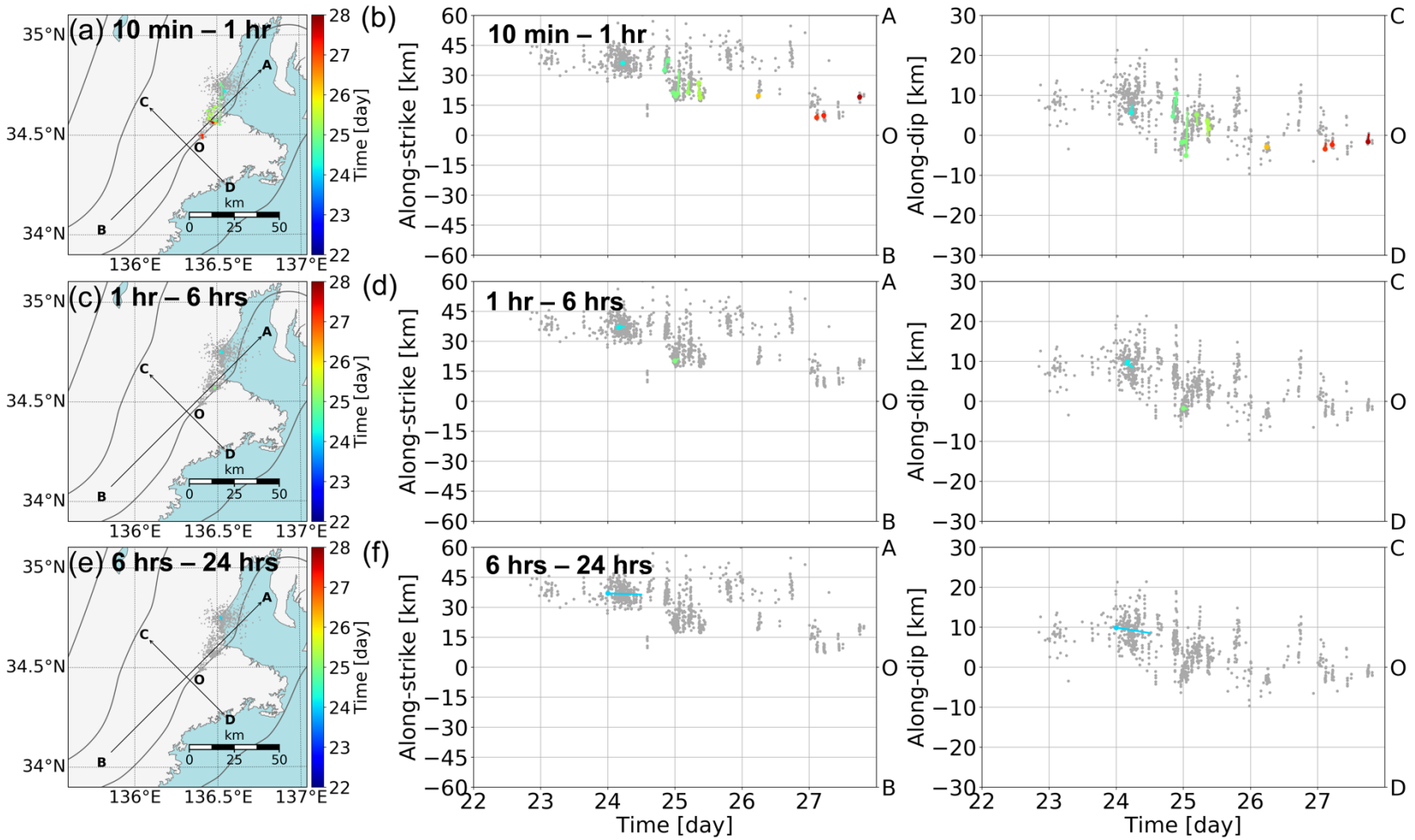

Figure S9. Same as Figure S2, but for tremor episode from January 22nd to 27th, 2014.

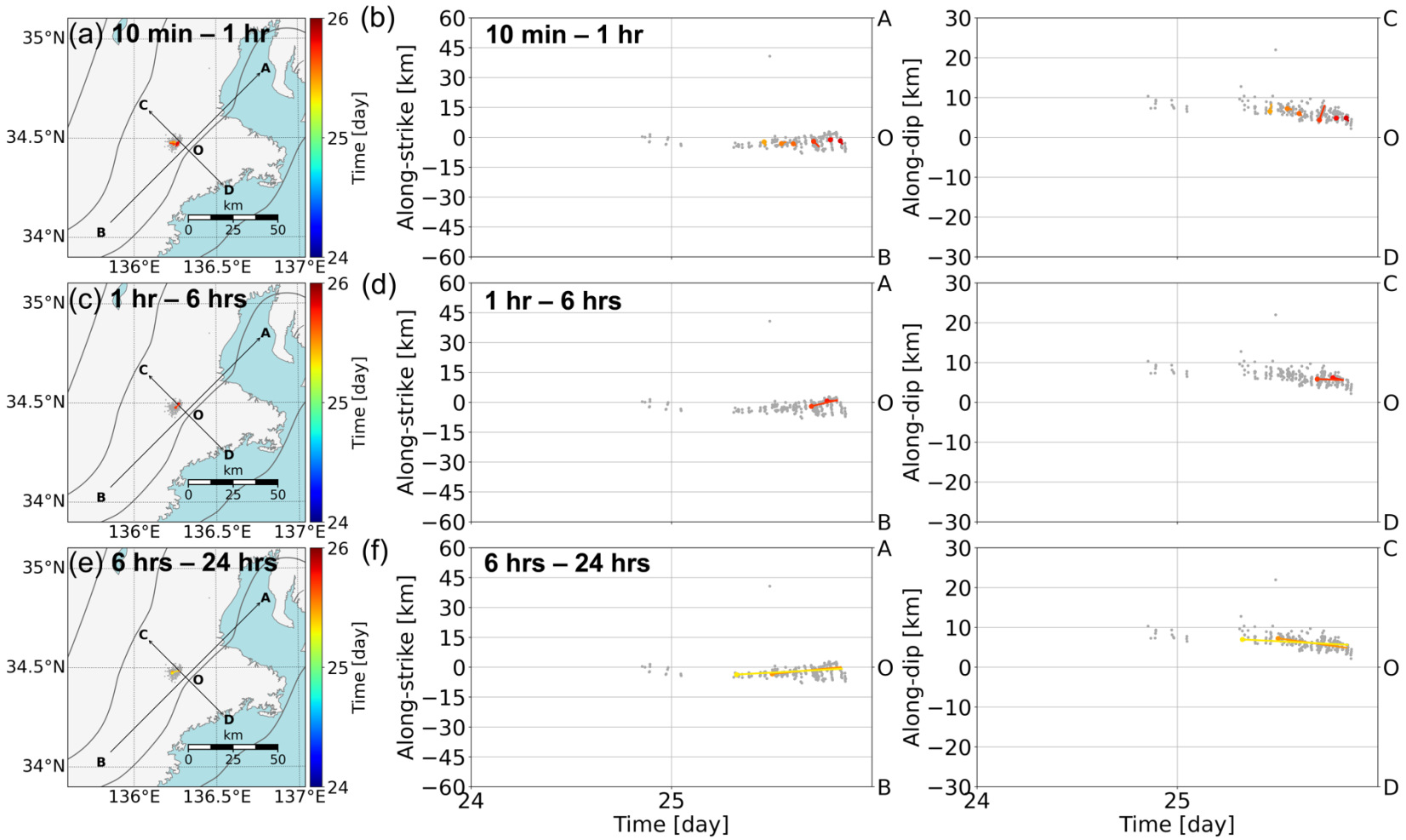

Figure S10. Same as Figure S2, but for tremor episode from April 24th to 25th, 2014.

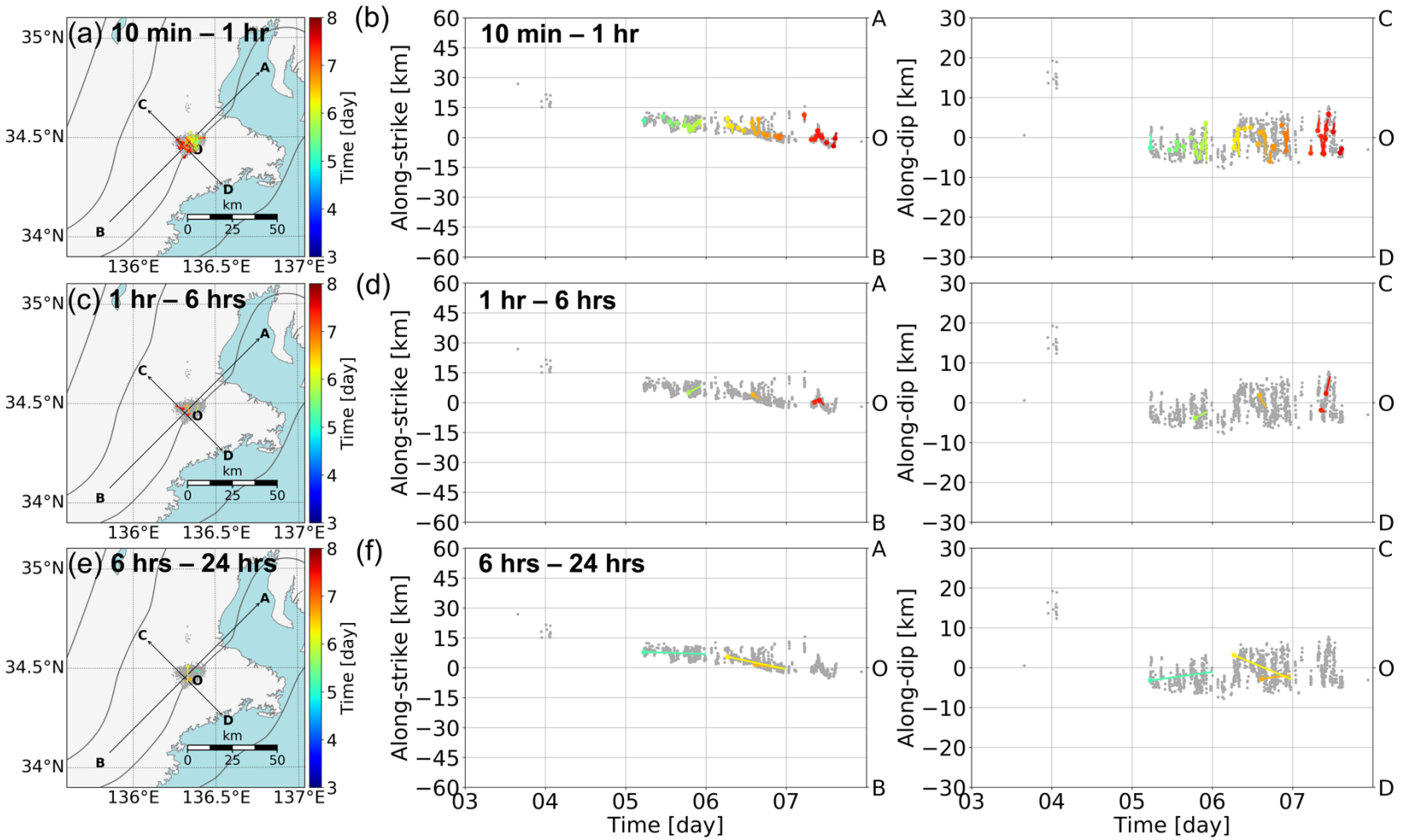

Figure S11. Same as Figure S2, but for tremor episode from May 3rd to 7th, 2014.

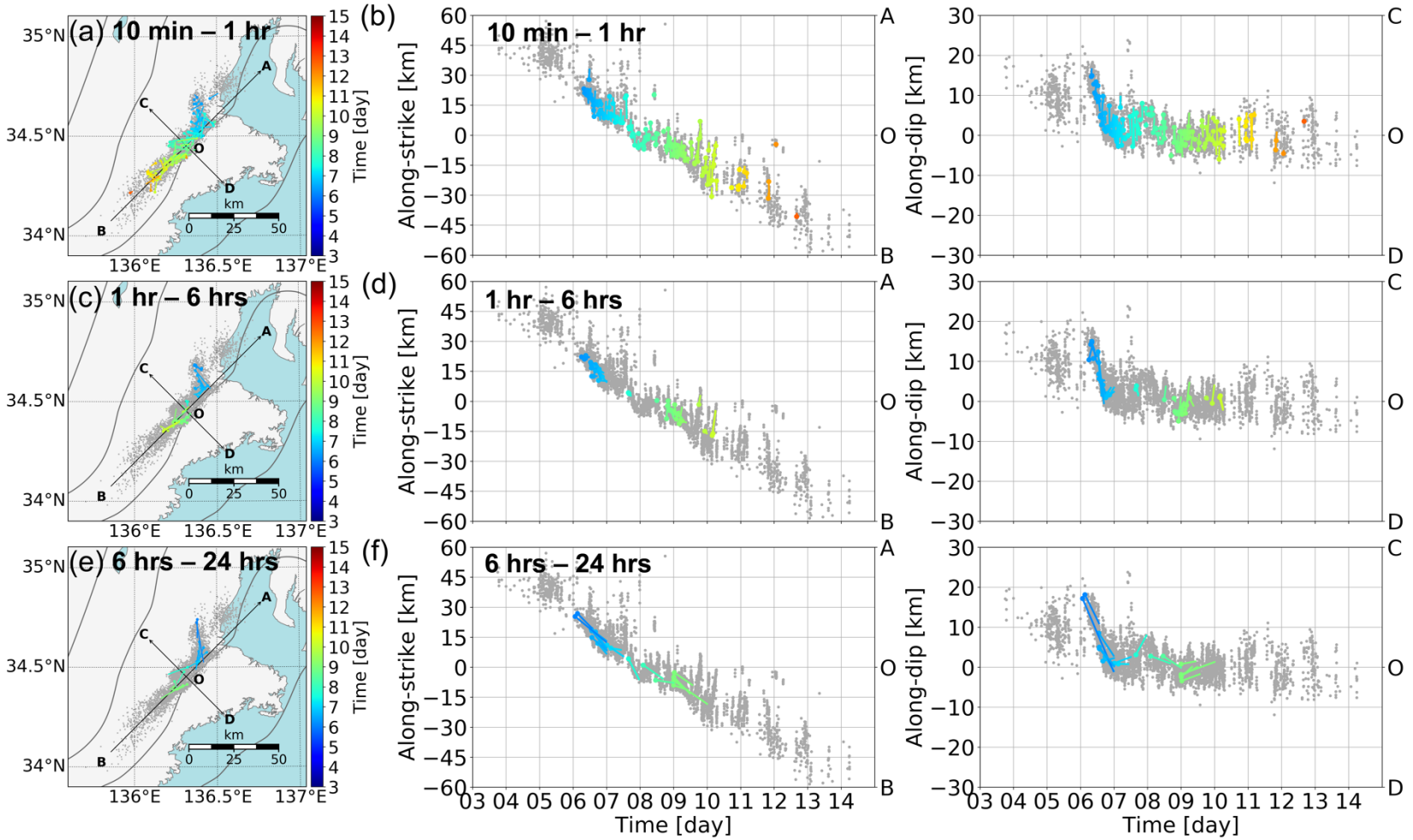

Figure S12. Same as Figure S2, but for tremor episode from July 3rd to 14th, 2014.

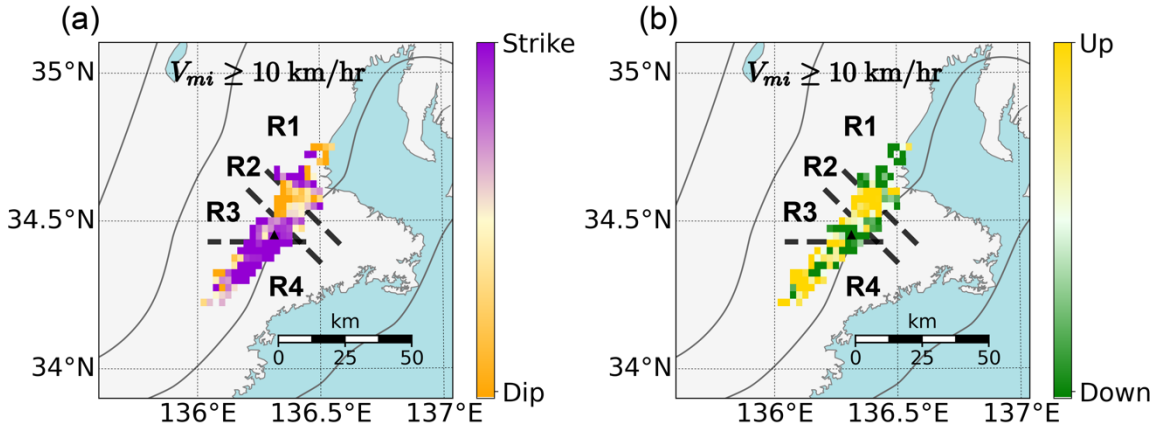

Figure S13. (**a**) Spatial distribution of predominant directions of tremor migrations with speeds of 10 km/hr or more. The black triangle shows the location of the array. The dashed lines are drawn to distinguish the areas R1–R4, where the frequency of tremor events composing tremor migrations is high. The violet color shows that tremor migrations along the strike are predominant (0–90° and 180–270° clockwise from the north), and the orange color shows that tremor migrations along the dip are predominant (90–180° and 270–360°). (**b**) Spatial distribution of predominant directions of tremor migrations with high speeds along the dip. The yellow and green colors show predominant directions of the up-dip (90–180°) and down-dip (270–360°), respectively.

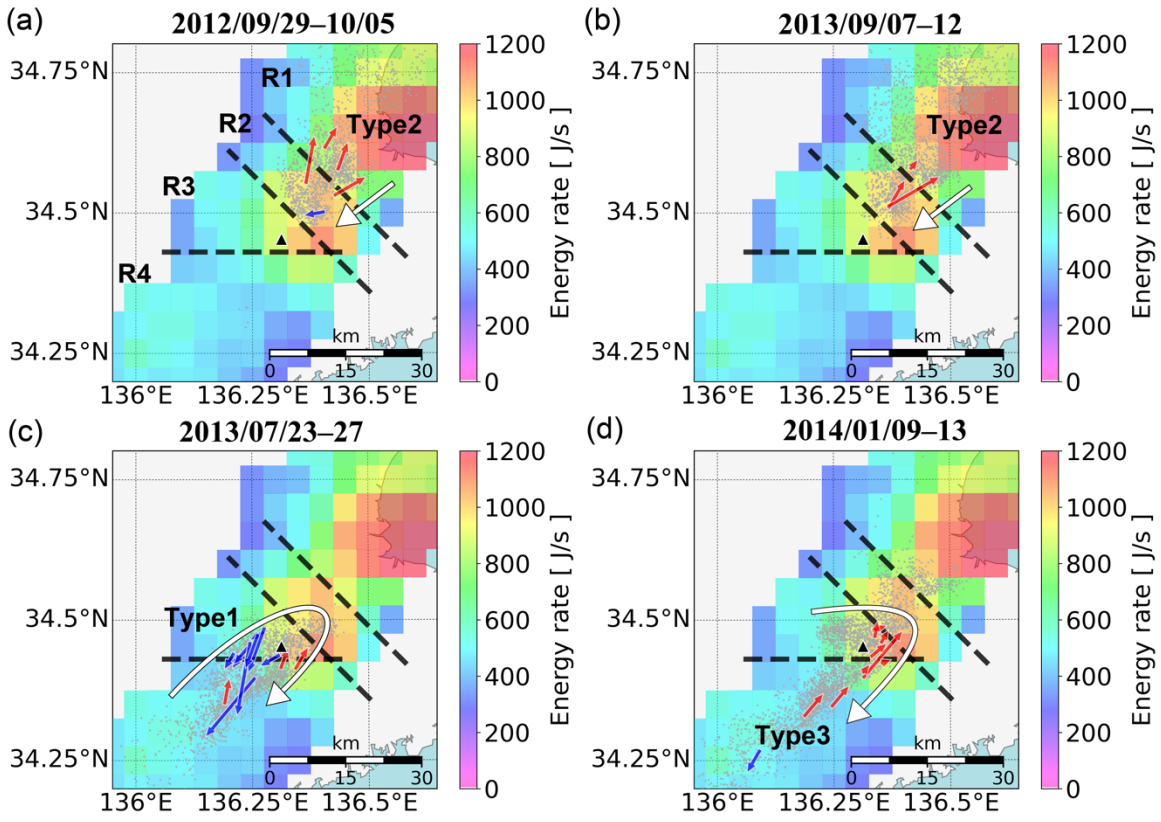

Figure S14. (**a**) Spatial distribution of RTRs during a tremor episode from September 29th to October 5th, 2012. The red arrows show RTRs propagating northeastward, and the blue arrows show those propagating southwestward. The white arrow shows the pattern of the main front and the gray dots show tremor locations. Type1–Type3 show different migration patterns of RTRs. The dashed lines and the black triangle are the same as Figure S13. The background colors show median energy rates (Yabe & Ide, 2014). (**b**) Same as (**a**), but for RTRs during a tremor episode from September 7th to 12th, 2013. (**c**) Same as (**a**), but for RTRs during a tremor episode from July 23rd to 27th, 2013. (**d**) Same as (**a**), but for RTRs during a tremor episode from January 9th to 13th, 2014.

Data Set S1. The catalog of tremor migrations extracted in the present study.
The data format is the followings: Year, Month, Day, Hour, starting time [min], ending time [min], longitude of starting point [deg], longitude of ending point [deg], latitude of starting point [deg], latitude of ending point [deg], ρ [km], migration speed [km/hr], ϕ [deg], and ψ [deg]. The starting time and ending time are elapsed time from Year-Month-Day Hour: 00:00. Time zone is Japan Standard Time (JST, UTC+9). ϕ is the migration direction measured counterclockwise from the east.